View metadata, citation and similar papers at core.ac.uk

brought to you by CORE

provided by Archivio della ricerca- Università di Roma La Sapienza

Applied Physics Letters

Cavitation bubble wall pressure measurement by an electromagnetic surface wave enhanced pump-probe configuration

Cite as: Appl. Phys. Lett. **114**, 134101 (2019); https://doi.org/10.1063/1.5089206
Submitted: 17 January 2019 . Accepted: 20 March 2019 . Published Online: 04 April 2019

Agostino Occhicone, Giorgia Sinibaldi, Norbert Danz, Carlo Massimo Casciola, and Francesco Michelotti

View Online Export Citation CrossMark

ARTICLES YOU MAY BE INTERESTED IN

Enhancement of resolution in microspherical nanoscopy by coupling of fluorescent objects to plasmonic metasurfaces
Applied Physics Letters **114**, 131101 (2019); https://doi.org/10.1063/1.5066080

Cavity-enhanced harmonic generation in silicon rich nitride photonic crystal microresonators
Applied Physics Letters **114**, 131103 (2019); https://doi.org/10.1063/1.5066996

The self-collimation effect induced by non-Hermitian acoustic systems
Applied Physics Letters **114**, 133503 (2019); https://doi.org/10.1063/1.5087162

© 2019 Author(s).

Applied Physics Letters ARTICLE scitation.org/journal/apl

Cavitation bubble wall pressure measurement by an electromagnetic surface wave enhanced pump-probe configuration

Cite as: Appl. Phys. Lett. **114**, 134101 (2019); doi: 10.1063/1.5089206
Submitted: 17 January 2019 · Accepted: 20 March 2019 ·
Published Online: 4 April 2019

View Online Export Citation CrossMark

Agostino Occhicone,[1,a)] Giorgia Sinibaldi,[2] Norbert Danz,[3] Carlo Massimo Casciola,[2] and Francesco Michelotti[1]

AFFILIATIONS

[1]Department of Basic and Applied Sciences for Engineering, SAPIENZA Università di Roma, via A. Scarpa, 16, 00161 Roma, Italy
[2]Department of Mechanical and Aerospace Engineering, SAPIENZA Università di Roma, via Eudossiana, 18, 00184 Roma, Italy
[3]Fraunhofer Institute for Applied Optics and Precision Engineering, A.-Einstein-Str. 7, 07745 Jena, Germany

[a)]Author to whom correspondence should be addressed: agostino.occhicone@uniroma1.it

ABSTRACT

We report on the measurement of the pressure associated with a shock wave within a very thin layer (100 nm) in proximity of a boundary surface. In the experiments, the shock wave was emitted by a cavitation bubble generated by a pulsed pump laser in water. We developed a pump-probe setup based on the detection of the light scattered at the surface of a one-dimensional photonic crystal, which was purposely designed to sustain a surface electromagnetic wave in the visible range and to enhance the optical response. In order to better understand the phenomenon, we implemented numerical simulations to describe the light scattering intensity distributions through a modified Rayleigh's method. We report, with a LoD of ∼0.1 MPa, the measurements of the pressure at a surface in the presence of a laser-induced cavitation bubble generated at different distances from the surface and for different pulse energies.

Published under license by AIP Publishing. https://doi.org/10.1063/1.5089206

In this work, we experimentally demonstrate a new pump-probe pressure sensing scheme exploiting the peculiar properties of surface electromagnetic waves (SEWs) sustained at the interface between a one-dimensional photonic crystal (1DPC) and water [Bloch surface waves (BSWs)]. We used the technique to reveal the pressure associated with the shock wave released by a cavitation bubble generated by a laser pulse (LP) in proximity of a boundary surface.

Bubbles' cavitation is one of the most discussed topics in fluid dynamics. Generally, it is associated with erosion damage,[1] but it is currently reconsidered for a wide range of modern applications in medicine,[2] microfluidics,[3] and other fields.[4] Accessing highly resolved pressure measurements at a boundary surface is of extreme interest to unveil the physical mechanisms governing the modification of cavitation bubble dynamics in proximity of the surface and could improve practical applications of cavitation bubbles, such as their interaction with endothelial barriers,[5] surfaces' cleaning,[6] and lithotripsy.[2]

The literature is rich of experimental works on bubbles' cavitation, in which the phenomenon is imaged by a fast camera and the associated pressure field is measured by means of a hydrophone, usually based on either an optical fiber probe (FOPH)[7–9] or a polyvinylidene piezoelectric film (PVDF). PVDF hydrophones are commonly used to carry out local pressure measurements at boundary surfaces, with the main advantage of resolving pressure changes better than the FOPH type. However, measuring the pressure field by means of such needle hydrophones, which typically have a diameter of 125–600 μm, involves embedding the needle in the boundary wall, with the sensitive tip at the surface. Under such conditions, the pressure field at the surface can be perturbed by the discontinuities at the needle tip. Moreover, mapping the field along the surface requires multiple needles, and more discontinuities would appear. The optical scheme proposed here permits us to measure the pressure field within a 100 nm thick layer at the surface with a transverse resolution on the order of 200 μm. In the experiments, we generated shock waves well inside water and detected their pressure upon their interaction with the 1DPC/water interface.

BSWs in the visible range[10] have been demonstrated recently to be very attractive and suitable for noninvasive measurements in proximity of a solid-fluid interface.[11,12] In the case of BSW, the solid is a

Published under license by AIP Publishing

dielectric multilayered structure characterized by a photonic bandgap, in which light propagation inside the 1DPC is forbidden. The localization of the BSW at the 1DPC/fluid interface is granted by Bragg and by total internal reflection (TIR), taking place at the 1DPC and the fluid medium sides, respectively.[13] The BSW field envelope decays exponentially on both sides. BSW can be excited by means of prism coupling in the Kretschmann-Raether total internal reflection (KR-TIR) configuration.[14]

In our experiments, the nucleation of bubbles was induced by a focused pulsed laser beam (pump).[4,15,16] The laser was a frequency-doubled Q-switched Nd:YAG-laser (Litron Nano S 35–15), which delivered laser pulses (LP) at the wavelength $\lambda_{pump} = 532$ nm, with a duration $\tau = 8$ ns, as well as tunable repetition rate and pulse energy up to f = 15 Hz and E = 30 mJ, respectively.

In order to get a highly symmetric laser-generated plasma,[3,4,15,17] the laser beam was first expanded (Galilean telescope with spherical lenses, focal lengths −25 and 200 mm) and then focused (spherical lens, focal length 75 mm) into a small volume with a relatively large numerical aperture (NA) = 0.21. Such a NA value reduces heating of water inside the laser beam in the proximity of the focal point.[4]

As shown in Fig. 1(a), the pulsed laser beam reached from top a transparent glass cavitation cuvette, which was 35 mm deep and 25 mm by 30 mm wide. One lateral facet of the cuvette was constituted by a 1DPC coated on a microscope slide. A system of mirrors and a micrometric mechanical stage permits us to change the distance of the focusing and the bubble nucleation point from the 1DPC surface. In the experiments, such a distance was about 1 cm.

Figure 1(b) shows sequences of video frames acquired by means of a fast camera (Photron FastCam mini UX100 fitted with an objective Nikon Micro-Nikkor 105 mm f/2.8G IF-ED) during the bubble nucleation experiments with a background illumination, when the pulse energy was either $E_{1,LP} = 27.0$ mJ or $E_{2,LP} = 29.1$ mJ. The fast camera was set to the framerate 80 kfps, i.e., one frame every 12.5 μs, and to a field of view 25.3×1.1 mm^2. From the first frame of both sets shown, we can see that, despite the large α value of the focusing angle, at both the energy levels, the plasma was extended and more than one plasma spot was visible. At $E_{1,LP}$, the series of frames showed the nucleation of a single bubble that then collapsed with an asymmetric shape. Increasing the LP energy to $E_{2,LP}$, the effects on the plasma shape were more pronounced and the bubble lost its symmetry.[18] Two well separated plasma spots were visible, and two bubbles were formed, which then grew and coalesced, but with a final asymmetric

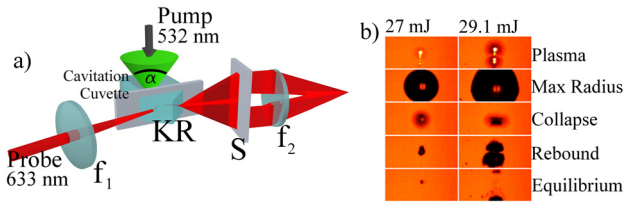

FIG. 1. (a) Sketch of the BSW based optical detection set-up. The light source is a He-Ne laser at 632.8 nm. The light is σ polarized and focused with a lens, f_1, on the 1DPC through the KR-TIR configuration. The reflected light was stopped through a slit (S) and the scattered light was collected by a lens, f_2, that focuses on the photodiode. (b) Video frames acquired for two LP energy levels: 27.0 mJ and 29.1 mJ. The videos were acquired at a frame rate of 80 kfps.

shape. The resulting bubble reached its maximum radius, and, at the collapse, it assumed the shape of an "eight"; at the end of the process, two residual bubbles were formed.

The 1DPC used in the experiments was deposited on standard glass microscope slides by plasma ion assisted evaporation (PIAD) under high vacuum conditions by means of an APS904 coating system (Leybold Optics). The dielectric materials used were SiO_2 (silica), Ta_2O_5 (tantala), and TiO_2 (titania). The deposition rates were 0.5 nm/s for SiO_2, 0.4 nm/s for Ta_2O_5, and 0.25 nm/s for the TiO_2 layer.[19] As shown in Fig. 2(a), the multilayer stack was formed by a repetitive unit with thicknesses $d_{SiO_2} = 275$ nm and $d_{Ta_2O_5} = 120$ nm (two period and half) and topped by two titania and silica thin layers that were both 20 nm thick. The refractive indices of the layers at $\lambda_{probe} = 632.8$ nm are (TiO_2) $2.293 + i1.83 \times 10^{-3}$, ($SiO_2$) $1.447 + i5 \times 10^{-6}$, and ($Ta_2O_5$) $2.075 + i5 \times 10^{-5}$.

As shown in Fig. 1(a), the back face of a 1DPC coated slide was coupled to a BK7 glass prism by means of an optical contact oil. The free surface of the 1DPC is used as a side facet of the transparent cavitation cuvette, allowing us to keep the 1DPC in contact with water, where the bubbles and pressure waves are generated.

Figure 1(a) shows the optical configuration used to excite the probe BSW. The beam emitted by a CW He-Ne laser at $\lambda_{probe} = 632.8$ nm is linearly polarized along the σ direction and is focused onto the 1DPC by means of a spherical lens ($f_1 = 150$ mm) through the BK7 coupling prism in the KR-TIR configuration and sensing local refractive index changes. A θ-2θ rotation stage allows us to set the probe beam incidence angle θ_i and the detection angle θ_d. When $\theta_i = \theta_{BSW}$, a BSW is resonantly excited at the interface between the 1DPC and water. For the present 1DPC design, the penetration depth of the BSW exponential tail in water is $\xi \sim 100$ nm and the BSW propagates along the surface for coupling distance $\delta \sim 200$ μm before being out-coupled in the prism.[20] Such a condition permits us to sense pressure changes in a water volume with extension $\delta \cdot \xi \cdot \eta$, where η is the focal spot size that is on the order of few tens of micrometers.

With reference to Fig. 2(a), the reflected beam is constituted by two components: the specularly reflected beam at θ_r and an m-line at θ_s due to scattering of the BSW [see Eqs. (II.1) and (II.2), respectively, in the supplementary material]. The specularly reflected light is filtered out by a beam stop, whereas the m-line is transmitted by a slit (S) and collected by a second spherical lens ($f_2 = 50$ mm) that focuses onto a photodetector. The slit provides an angular resolution of ∼0.09°. The voltage signal V_p at the photodetector was acquired with an oscilloscope (Tektronix 2440) that was controlled by a computer through a LabView VI.

In Figs. 2(b) and 2(c), we show the results of the numerical calculations obtained for the two reflected components and carried out by means of a modified Rayleigh's method, which was already applied to BSW and discussed in Refs. 21 and 22 (details in the supplementary material). As sketched in Fig. 2(a), for the sake of simplicity, we assumed that the roughness is localized just at the last 1DPC interface (see Figs. S1 and S2 in the supplementary material). In a real system, natural roughness may exist at all interfaces. However, we expect that roughness at multiple interfaces produces an overall change of the scattered intensity but that the structure of the angular spectra remains unmodified.[23] The roughness is modeled by a surface function f(y), which is assumed to be continuous, stationary, and characterized by a

Published under license by AIP Publishing

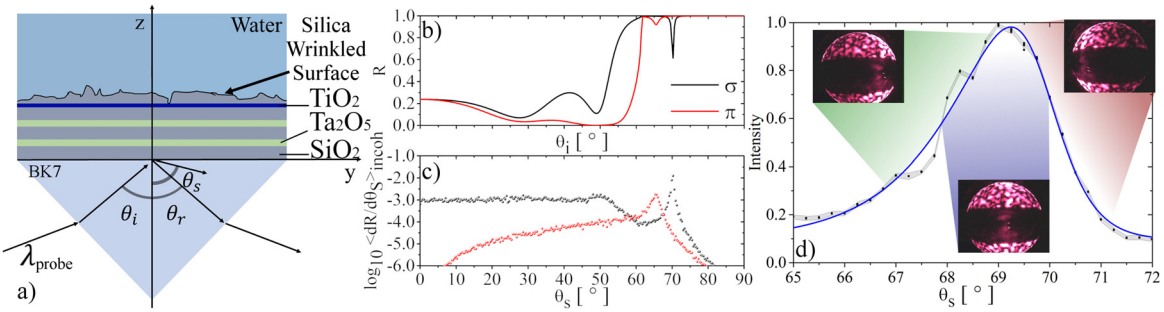

FIG. 2. (a) 1DPC with a rough surface placed between two semi-infinite homogeneous media. The wave with wavelength λ_{probe} impinges with an angle θ_i through the BK7 entrance material and is scattered at an angle θ_s. (b) Reflection profiles when a polarized light beam, σ (black) and π (red), and wavelength λ_{probe} impinge on the 1DPC. (c) Scattering from the BSW excited on top of the 1DPC when the polarized light impinges to an angle $\theta_i = 69°$. (d) Measurement set-up calibration. The plot of the signal normalized to 1 as a function of the detection angle, θ_d. The insets show photos of the reflected probe beam profile.

random Gaussian distribution with correlation length ξ_c.[21] In the calculations reported here, we used a root mean square value $f_{rms} = f_{rms,0} = \lambda_{probe}/16\,000$ and $\xi_c = \lambda_{probe}/5$ (calculation details are in the supplementary material).

Figure 2(b) shows the calculated specular reflectance component at λ_{probe} as a function of $\theta_i = \theta_r$, for both the σ and the π polarizations. The angular reflectance spectra show dips situated beyond the TIR edge (about 62°), which are due to the excitation, absorption, and scattering of a BSW. The results obtained with the Rayleigh's method confirm those obtained by means of the transfer matrix method[24] (see Fig. S3 in the supplementary material). In particular, in the σ case which is used here, the BSW resonance is at $\theta_i = 70.142°$ at λ_{probe}.[19]

Figure 2(c) shows the distribution of the scattered component of the reflected light as a function of θ_s for both the σ and the π polarization, when the excitation angle is set at $\theta_i = 69°$. Scattering peaks around the angles corresponding to the BSW dips shown in Fig. 2(b). Tuning θ_i around the BSW resonance leads to an overall change of the scattering intensity, without any change of the shape of the curves (see Fig. S4 in the supplementary material). In the experiments, θ_i was always set at resonance.

The angular position of the BSW resonances may change due to any perturbation of the refractive index of the liquid at the 1DPC surface (see Figs. S5 and S6 in the supplementary material). In particular, for pressure induced changes, the sensitivity S_p of the setup can be decomposed into the product of several terms

$$S_p = \frac{\partial V_p}{\partial p} = \frac{\partial V_p}{\partial \theta_{BSW}} \cdot \frac{\partial \theta_{BSW}}{\partial n} \cdot \frac{\partial n}{\partial p}. \quad (1)$$

At atmospheric pressure, we found $\partial n/\partial p = 1.49 \times 10^{-4}\,\mathrm{MPa}^{-1}$.[25] $\partial\theta_{BSW}/\partial n$ is the 1DPC bulk sensitivity, defined as the angular shift of the BSW resonances shown in Figs. 2(b) and 2(c) in response to a refractive index perturbation. For small perturbations, the variation of the amplitude and width of the BSW resonance can be neglected. We experimentally measured $\partial\theta_{BSW}/\partial n = 34°/\mathrm{RIU}$, for the σ polarization.[11] The term $\partial V_p/\partial\theta_{BSW}$ has a strong nonlinear dependency on θ_d. In order to evaluate such a term, we implemented a calibration measurement. We set $\theta_i = \theta_{BSW}$ with the cavitation cuvette filled with pure water. The photodiode voltage V_p was acquired for several different θ_d. The results are plotted in Fig. 2(d). In the insets, we show some images of the scattering pattern over an angular range of ~2°, recorded without slit S by a CMOS camera placed between the collecting lens f_2 and the photodetector. From the fit with an asymmetrical peak function, we experimentally found the BSW resonance, $\theta_{BSW} = 69.2° \pm 0.2°$ and the full width at half maximum (FWHM) equal to $2.4° \pm 0.1°$.

From Fig. 2(d), it is simple to show that the best condition to operate is setting θ_d at the FWHM angle, where the local slope of the curve is maximum. Under these conditions, for $\theta_d = 70.1°$, the maximum sensitivity S_p is evaluated to be $(1.2 \pm 0.5) \times 10^{-4}$ V/MPa. The voltage signals measured by the photodiode could be therefore converted to pressure signals by using S_p.

The temporally resolved pressure signals recorded with the BSW pump-probe setup are plotted as a function of time for several different bubble nucleation positions and pump laser pulse energies in Figs. 3(a) and 3(b), respectively. Each plot shown in Fig. 3 was obtained by averaging 128 cavitation events. The curves were obtained by subtracting the background signal acquired during a measurement with the probe beam stopped. The acquired signals were then smoothed by means of a local 2nd order polynomial regression method around each point [Savitzky-Golay filter (SG-f)], giving rise to the curves shown. The latter method preserves the features of the data, such as peak height and width. For the best smoothness of the result, the number of data points used in each local regression was 150.

Furthermore, from the acquired data, we evaluated the limit of detection (LoD) of our pump-probe system as the noise level on the measurements, δV. It is calculated as the standard deviation of a time dependent signal obtained under stationary conditions, i.e., in the absence of pressure sources inside the water volume, and then is converted to a pressure value by the sensitivity S_p. We evaluated the LoD as one standard deviation of the measurement noise in a 10 μs window for the following cases:

1. single cavitation event, $\mathrm{LoD}_1 = 5$ MPa;
2. average of 128 events, $\mathrm{LoD}_{128} = 0.3$ MPa;
3. average of 128 events and SG filtering as described above, $\mathrm{LoD}_{SG\text{-}f} = 0.1$ MPa.

The LoD_1 value should be compared to the LoD of commercial FOPH (around 0.5 MPa, 100 MHz bandwidth),[26] which makes use of dedicated electronics for signal conditioning that was not used in our case and that could improve the LoD_1 value.

Published under license by AIP Publishing

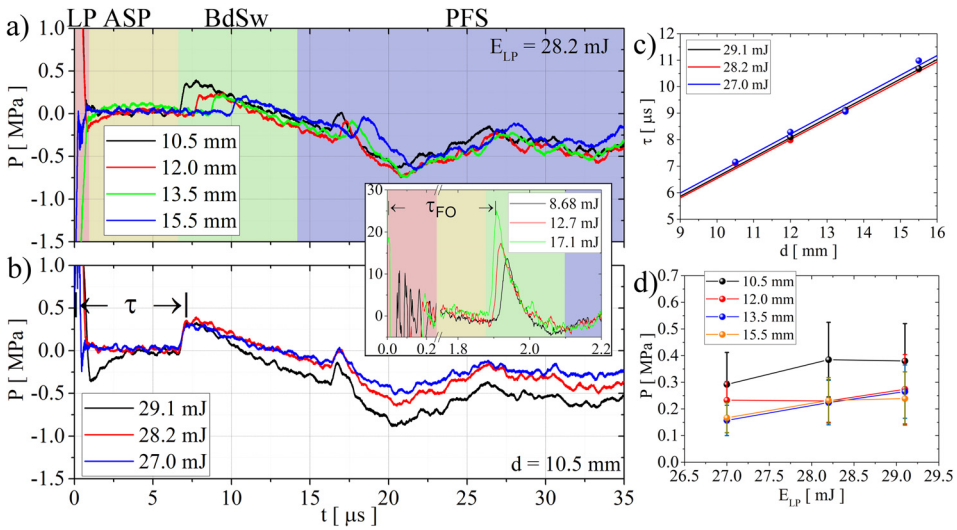

FIG. 3. (a) Measured pressure when the cavitation bubble position is tuned, and the laser pulse energy is fixed to 28.2 mJ. The different background colors highlight the different phases of the bubble cavitation. (b) Measured pressure when the laser pulse energy is tuned, and the bubble nucleation position is fixed to a distance from the 1DPC surface equal to 10.5 mm. In the inset, we show the pressure measured by a classical FOPH when the pressure shock waves are collected for different laser pulse energies. (c) BdSw temporal position vs bubble nucleation position. (d) BdSw pressure peak value vs the pulsed laser energy.

In Figs. 3(a) and 3(b), the acquired signals are triggered on the LP (0 μs). After an acoustically silent period (ASP), the BSW probe senses a first shock pulse that we associate with the breakdown shock wave (BdSw), followed by an oscillating signal related to the pressure fluctuations (PFS). Such regions are highlighted in Fig. 3(a). As a reference, in the inset of Fig. 3, we show the pressure measurement provided by a custom FOPH averaging over 256 cavitation events ($LoD_1 = 10$ MPa, with the same acquisition electronics and the same level of noise) for a free laser induced cavitation bubble.[4,18] The BdSw is centered to $\tau_{FO} \sim 2$ μs ($\sim$3 mm far from the bubble nucleation point) and the signals are obtained for laser pulse energies comparable with the energy used to nucleate the bubble in the case of the measurements with the BSW hydrophone.

The measurements shown in Fig. 3(a) were obtained for the same $E_{LP} = 28.2$ mJ and for the following distances d of the bubble nucleation point from the 1DPC surface: 15.5 mm, 13.5 mm, 12.0 mm, and 10.5 mm. We observe that the BdSw signals are delayed for bubbles generated farer from the 1DPC surface. In Fig. 3(c), we plot the BdSw delay τ as a function of d, as defined in Fig. 3(b) by the arrows. As expected, τ scales linearly with d. The inverse of the slope of the linear fit provides an evaluation of the speed of sound in water. We found 1370 ± 60 m/s, in good agreement with the values reported in the literature.[27] The BdSw signals show a rise time of about 40 ns and a very long fall time ($\sim$2.3 μs). The latter is in contrast to the results reported in the literature[15,28] and with what we observed with a FOPH (inset of Fig. 3), where the width of the peak associated with the BdSw is few tenths of nanoseconds. The long fall time, together with the negative sloped trend and the superimposed modulation, is probably artifacts introduced by the signal averaging procedures.

The measurements shown in Fig. 3(b) were obtained for three different LP energies when the bubble nucleation point was fixed to $d = 10.5$ mm. We observe that the pressure peak associated with the BdSw does not change its delay τ. The amplitude of the response shows a slight positive trend, as shown in the plot of Fig. 3(d), which, however, cannot be resolved in the limit of the error.

From the pressure signals plotted in Figs. 3(a) and 3(b), in the PFS region, we can observe that the fluctuations were located always at the same temporal delay from the first BdSw of about 8 μs. Taking into account the sound speed in water and the covered distance, we can associate the origin of these peaks with the pressure wave reflected by the lateral walls of the cavitation cuvette. Moreover, Fig. 3(b) illustrates that such fluctuations depend on the LP energy: they are larger when increasing the LP energy.

In conclusion, we proposed a surface enhanced pump-probe configuration for the characterization of the temporal evolution of the pressure at a surface with a competitive sensitivity, allowing us to study cavitation of bubbles with diameters on the order of 1 or 2 mm by measuring pressures that are some tenths of MPa. The system supplies a limit of detection (LoD) on the order of $\sim$5 MPa for measurements of single cavitation events; it reaches a LoD of $\sim$0.1 MPa when averaging over 128 single cavitation event signals and after a denoise signal postprocess.

See supplementary material for the mathematical model used to calculate the intensity of the light scattered by a 1DPC when a BSW is excited on its surface. We show how the scattered light intensity depends on the 1DPC roughness surface and on the light incidence angle.

This work was partially funded by the Regione Lazio (Italy), Programme "Progetti di Gruppi di Ricerca", funded project TURNOFF (85-2017-14945) and by the European Research Council under the European Union's Seventh Framework Programme (FP7/ 2007-2013)/ ERC Grant agreement no. (339446).

REFERENCES

[1] M. S. Plesset and R. E. Devine, "Effect of exposure time on cavitation damage," J. Basic Eng. **88**(4), 691–699 (1966).
[2] C. E. Brennen, "Cavitation in medicine," Interface Focus **5**(5), 20150022 (2015).
[3] E. Zwaan, S. Le Gac, K. Tsuji, and C. D. Ohl, "Controlled cavitation in microfluidic systems," Phys. Rev. Lett. **98**(25), 254501 (2007).
[4] D. Obreschkow, M. Tinguely, N. Dorsaz, P. Kobel, A. de Bosset, and M. Farhat, "The quest for the most spherical bubble: Experimental setup and data overview," Exp. Fluids **54**, 1503 (2013).
[5] G. Peruzzi, G. Sinibaldi, G. Silvani, G. Ruocco, and C. M. Casciola, "Perspectives on cavitation enhanced endothelial layer permeability," Colloid Surf., B. **168**, 83–93 (2018).

Published under license by AIP Publishing

[6]C. D. Ohl, M. Arora, R. Dijkink, V. Janve, and D. Lohse, "Surface cleaning from laser-induced cavitation bubbles," Appl. Phys. Lett. **89**(7), 074102 (2006).
[7]J. Staudenraus and W. Eisenmenger, "Fibre-optic probe hydrophone for ultrasonic and shock-wave measurements in water," Ultrasonics **31**(4), 267–273 (1993).
[8]J. E. Parsons, C. A. Cain, and J. B. Fowlkes, "Cost-effective assembly of a basic fiber-optic hydrophone for measurement of high-amplitude therapeutic ultrasound fields," J. Acoust. Soc. Am. **119**(3), 1432–1440 (2006).
[9]W. Lauterborn, T. Kurz, C. Schenke, O. Lindau, and B. Wolfrum, "Laser-induced bubbles in cavitation research," in *IUTAM Symposium on Free Surface Flows*, Fluid Mechanics and Its Applications Vol. 62 (Springer, 2001), pp. 169–176.
[10]P. Yeh, A. Yariv, and C.-S. Hon, "Electromagnetic propagation in periodic stratified media. I. General theory," J. Opt. Soc. Am. **67**(4), 423–438 (1977).
[11]A. Occhicone, A. Sinibaldi, F. Sonntag, P. Munzert, N. Danz, and F. Michelotti, "A novel technique based on Bloch surface waves sustained by one-dimensional photonic crystals to probe mass transport in a microfluidic channel," Sens. Actuator, B. **247**, 532–539 (2017).
[12]A. Sinibaldi, C. Sampaoli, N. Danz, P. Munzert, L. Sibilio, F. Sonntag, A. Occhicone, E. Falvo, E. Tremante, P. Giacomini, and F. Michelotti, "Detection of soluble ERBB2 in breast cancer cell lysates using a combined label-free/fluorescence platform based on Bloch surface waves," Biosens. Bioelectron. **92**, 125–130 (2017).
[13]A. P. Vinogradov, A. V. Dorofeenko, A. M. Merzlikin, and A. A. Lisyansky, "Surface states in photonic crystals," Physics-Uspekhi **53**(3), 243–256 (2010).
[14]H. Raether, *Surface Plasmons on Smooth and Rough Surfaces and on Gratings* (Springer, Berlin, 1986).
[15]W. Lauterborn and A. Vogel, "Shock wave emission by laser generated bubbles," Bubble Dyn. Shock Waves **8**, 67–103 (2013).
[16]A. Vogel, J. Noack, K. Nahen, D. Theisen, S. Busch, U. Parlitz, D. X. Hammer, G. D. Noojin, B. A. Rockwell, and R. Birngruber, "Energy balance of optical breakdown in water at nanosecond to femtosecond time scales," Appl. Phys. B **68**, 271–280 (1999).
[17]C. D. Ohl, T. Kurz, R. Geisler, O. Lindau, and W. Lauterborn, "Bubble dynamics, shock waves and sonoluminescence," Philos. Trans. R. Soc. London, A **357**(1751), 269–294 (1999).
[18]G. Sinibaldi, A. Occhicone, F. A. Pereira, D. Caprini, L. Marino, F. Michelotti, and C. M. Casciola, "Laser induced breakdown and bubble cavitation," in *Proceeding of CAV2018* (2018), p. 05137.
[19]A. Anopchenko, A. Occhicone, R. Rizzo, A. Sinibaldi, G. Figliozzi, N. Danz, P. Munzert, and F. Michelotti, "Effect of thickness disorder on the performance of photonic crystal surface wave sensors," Opt. Express **24**(7), 7728–7742 (2016).
[20]A. Sinibaldi, A. Fieramosca, N. Danz, P. Munzert, A. Occhicone, C. Barolo, and F. Michelotti, "Effects of reabsorption due to surface concentration in highly resonant photonic crystal fluorescence biosensors," J. Phys. Chem. C **122**(45), 26281–26287 (2018).
[21]R. G. Llamas, L. E. Regalado, and C. Amra, "Scattering of light from two-layer system with a rough surface," J. Opt. Soc. Am., A **16**(11), 2713–2719 (1999).
[22]A. Sentenac and J. J. Greffet, "Mean-field theory of light scattering by one-dimensional rough surfaces," J. Opt. Soc. Am., A **15**(2), 528–532 (1998).
[23]A. S. R. Duverger, J. G. Armenta, and R. G. Llamas, "Surface wave effect on the light scattering from one-dimensional photonic crystals," Opt. Commun. **277**(2), 302–309 (2007).
[24]A. Sinibaldi, R. Rizzo, G. Figliozzi, E. Descrovi, N. Danz, P. Munzert, A. Anopchenko, and F. Michelotti, "A full ellipsometric approach to optical sensing with Bloch surface waves on photonic crystals," Opt. Express **21**(20), 23331–23344 (2013).
[25]A. Arvengas, K. Davitt, and F. Caupin, "Fiber optic probe hydrophone for the study of acoustic cavitation in water," Rev. Sci. Instrum. **82**(3), 034904–034908 (2011).
[26]See http://www.ondacorp.com/products_HFO.shtml for noise equivalent pressure.
[27]*CRC Handbook of Chemistry and Physics*, 89th ed., edited by D. R. Lide and B. Raton (CRC Press/Taylor and Francis Group, 2009), p. 2736.
[28]G. N. Sankin, Y. Zhou, and P. Zhong, "Focusing of shock waves induced by optical breakdown in water," J. Acoust. Soc. Am. **123**(6), 4071–4081 (2008).

Published under license by AIP Publishing